Experimental demonstration of two-photon Mueller matrix second-harmonic generation microscopy

Chukwuemeka Okoro
Kimani C. Toussaint, Jr.

Experimental demonstration of two-photon Mueller matrix second-harmonic generation microscopy

Chukwuemeka Okoro[a] and Kimani C. Toussaint Jr.[b,c,]*
[a]University of Illinois at Urbana–Champaign, PROBE Lab, Department of Electrical and Computer Engineering, 1206 W Green Street, Urbana, Illinois 61801, United States
[b]University of Illinois at Urbana–Champaign, PROBE Lab, Department of Mechanical Science and Engineering, 1206 W Green Street, Urbana, Illinois 61801, United States
[c]University of Illinois at Urbana–Champaign, PROBE Lab, Affiliate in the Department of Electrical and Computer Engineering and Bioengineering, 1206 W Green Street, Urbana, Illinois 61801, United States

Abstract. We present the first experimental demonstration of two-photon Mueller matrix second-harmonic generation (SHG) microscopy for the extraction of representative Mueller matrices. Individual SHG images of porcine sample sets are divided into subimages, and the local nonlinear two-photon Mueller matrices ($M^{(2)}$) and degree of polarization (p) are determined. Results of the two-photon Mueller matrices from different sample types and the effects of thickness on the mean p distribution per polarization basis are investigated. We find that the p distribution shape changes and an associated bimodal mean difference (μ_d) increases with thickness. Our approach has potential as a quantitative imaging technique and can be applied to other multiphoton coherent imaging modalities. © *2016 Society of Photo-Optical Instrumentation Engineers (SPIE)* [DOI: 10.1117/1.JBO.21.1.016011]

1 Introduction

Assessment of the structural organization of collagen fibers in tissues could help elucidate structure-function mechanisms, which will be important to mechanobiology as well as biomedical research areas ranging from reproductive health[1] to cancer studies.[2] This is made more relevant by the ubiquitousness of collagen as the most prevalent protein in the human body.[3] The noncentrosymmetric structure of collagen makes it an excellent candidate for second-harmonic generation (SHG) imaging. Indeed, owing to the fact that SHG is a second-order nonlinear optical scattering process, it has been shown that SHG imaging of fibrillar collagen-based tissues results in high-contrast images with submicron three-dimensional (3-D) spatial resolution.[4]

Several quantitative techniques have been applied in order to assess collagen organization. An example is the forward-to-backward intensity ratio (F/B), which has been used to highlight differences in morphology between various tissues.[5,6] Another approach is the Fourier-transform (FT) SHG method employed to determine the 3-D structural organization of collagen fibers.[7,8]

Polarization-resolved (PR) methods for SHG[9] and sum-frequency generation,[10] have also been used to investigate the optical anisotropic properties of collagen. The d-ratio analysis, which involves the second-order susceptibility d-parameters, has been used in studies of melanoma tumor tissues[11] and breast tissue microarrays having different pathological conditions.[2] Notwithstanding the potential utility of this approach, methods employing extraction of these d-parameters are hampered by the requirement to accurately model the biological tissue, often with some particular crystallographic symmetry. Therefore, a quantitative imaging approach that utilizes well-known polarimetric methods based on a Mueller calculus would be attractive to SHG imaging since it obviates the need to have the aforementioned tissue model. The Mueller matrix can be considered a transformation from an input to an output Stokes vector representation of light, which allows one to describe the polarization altering behavior of an optical system by a matrix.[12]

As a metrology technique, Mueller matrix polarimetry, or a similar variant, has been previously adapted to multiphoton imaging. For example, Mazumder et al.[13] presented a technique of illuminating a sample with different polarization states to obtain the Stokes parameters, and subsequently extract both a degree of polarization and an anisotropy ratio as quantitative metrics. In addition, Ávila et al.[14] acquired sets of SHG images of cornea and sclera for independent polarization states, and used the Mueller matrix elements to reconstruct the images for contrasting quality metrics. However, these techniques relate the linear Mueller matrix model to the nonlinear SHG process, and thus an interpretation of the measured results is not clear. Fortunately, Shi et al.[15] showed that the standard, one-photon, Mueller calculus used in linear optics can be extended to a general two-photon case through the use of a so-called double Mueller matrix. In this manuscript, we experimentally demonstrate two-photon Mueller Matrix (MM$^{(2)}$)-SHG microscopy by applying the double Mueller matrix polarimetry to SHG imaging. Specifically, we show that measurement of the output Stokes vector permits an estimation of the Mueller matrix for unstained porcine tendon and skin, in principle, down to the level of a single pixel. We also use the Stokes vector to determine the degree of polarization of the nonlinear output.

*Address all correspondence to: Kimani C. Toussaint, E-mail: ktoussai@illinois.edu

2 Theory

The Stokes vector used in linear optics describes the polarization state of light in a 4×1 vector form[16] and can be expressed as $\begin{pmatrix} I_H + I_V & I_H - I_V & I_P - I_{P^*} & I_R - I_{R^*} \end{pmatrix}^T$, where I stands for the intensity and the subscripts H, V, P, P^*, R, and R^* represent 0 deg, 90 deg, 45 deg, and -45 deg, right-hand circularly polarized and left-hand circularly polarized light, respectively.

The one-photon Mueller matrix relationship between input (s_β) and output ($\tilde{s}_\alpha$) Stokes vectors is[15]

$$\tilde{s}_\alpha = M^{(1)}_{\alpha\beta} s_\beta \qquad \alpha, \beta = 0, 1, 2, 3, \tag{1}$$

where $M_{\alpha\beta}$ is a 4×4 Mueller matrix, the zero index is used for consistency with Stokes convention, and repeated subscripts imply summation over those subscripts. The Mueller calculus approach assumes a linear relation between the input and output Stokes vectors. In general, for a multiphoton effect, the Mueller matrix becomes an $(n + 1)$ dimensional array, where n is the order of the effect. For two-photon effects, Eq. (1) becomes
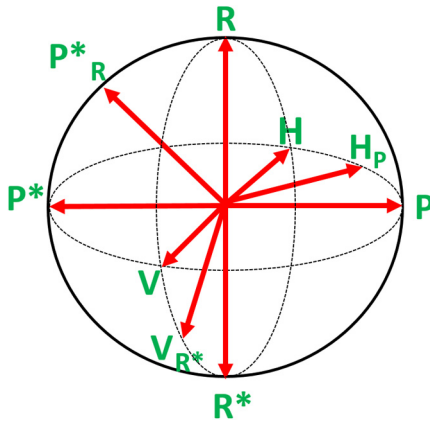
Fig. 1 Poincaré sphere representation of selected input states.

$$\tilde{s}_\alpha = M^{(2)}_{\alpha\beta\gamma} s_\beta s'_\gamma \qquad \alpha, \beta, \gamma = 0, 1, 2, 3, \tag{2}$$

where the $M^{(2)}_{\alpha\beta\gamma}$ is a $4 \times 4 \times 4$ two-photon Mueller array relating two input Stokes vector (s_β and s'_γ) to yield an output Stokes vector.

For the case of SHG having two input photons with the same energy, we can reduce the 3-D $4 \times 4 \times 4$ array operating on two 4×1 input vectors to a 4×9 matrix operating on one 9×1 input vector so that $M^{(2)}_{\alpha\beta\gamma} \Rightarrow M^{(2)}_{\alpha\Gamma}$ and

$$\tilde{s}_\alpha = M^{(2)}_{\alpha\Gamma} S_\Gamma \qquad \alpha = 0, 1, 2, 3 \quad \Gamma = 0, 1, 2, \dots, 8, \tag{3}$$

where S_Γ is the double Stokes representation and can be expressed in terms of single Stokes values as[17]

$$S_\Gamma = \begin{pmatrix} S_0 \\ S_1 \\ S_2 \\ S_3 \\ S_4 \\ S_5 \\ S_6 \\ S_7 \\ S_8 \end{pmatrix} = \begin{pmatrix} \sqrt{\frac{1}{6}}(3s_0^2 - s_1^2) \\ \sqrt{\frac{1}{12}}(5s_1^2 - 3s_0^2) \\ -s_0 s_1 \\ \frac{1}{2}(s_2^2 - s_3^2) \\ s_2(s_1 + s_0) \\ -s_2(s_1 - s_0) \\ -s_2 s_3 \\ s_3(s_1 + s_0) \\ s_3(s_1 - s_0) \end{pmatrix}. \tag{4}$$

A series of nine known input polarization states are generated. The first six are chosen on the convention for linear Stokes, while the other three are chosen such that they present a symmetric disposition with respect to the first six on the Poincaré sphere as shown in Fig. 1 (a slightly different model from Ref. 15).

For each input state, output images for the polarization analyzer settings should be acquired (that is, H, V, P, P^*, R, and R^*). Hence, the set of nine equations to solve are
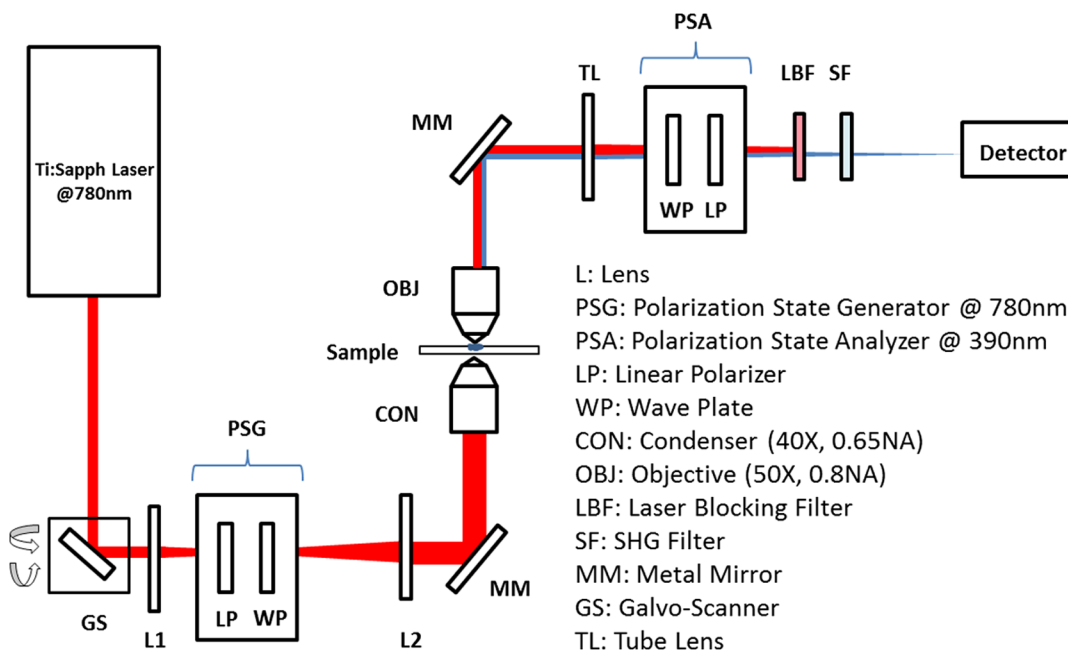
Fig. 2 Experimental setup for the image acquisition process.

L: Lens
PSG: Polarization State Generator @ 780nm
PSA: Polarization State Analyzer @ 390nm
LP: Linear Polarizer
WP: Wave Plate
CON: Condenser (40X, 0.65NA)
OBJ: Objective (50X, 0.8NA)
LBF: Laser Blocking Filter
SF: SHG Filter
MM: Metal Mirror
GS: Galvo-Scanner
TL: Tube Lens

$$M^{(2)} \cdot H^{(i)} = H^{(o)}, \quad M^{(2)} \cdot V^{(i)} = V^{(o)},$$
$$M^{(2)} \cdot P^{(i)} = P^{(o)}, \quad M^{(2)} \cdot P^{*(i)} = P^{*(o)},$$
$$M^{(2)} \cdot R^{(i)} = R^{(o)}, \quad M^{(2)} \cdot R^{*(i)} = R^{*(o)},$$
$$M^{(2)} \cdot H_P^{(i)} = H_P^{(o)}, \quad M^{(2)} \cdot V_{R^*}^{(i)} = V_{R^*}^{(o)},$$
$$M^{(2)} \cdot P_R^{*(i)} = P_R^{*(o)}, \tag{5}$$

where $M^{(2)}$ is the two-photon Mueller 4×9 matrix, the (i) superscript denotes input 9×1 two-photon Stokes vector, and (o) superscript stands for output 4×1 Stokes vector. The individual input and output matrices obtained for each polarization input can be concatenated to obtain consolidated 9×9 input $(U^{(i)})$ and 4×9 output $(U^{(o)})$ matrices, respectively, as

$$U^{(i)} = \begin{pmatrix} H^{(i)} & V^{(i)} & P^{(i)} & P^{*(i)} & R^{(i)} & R^{*(i)} & H_P^{(i)} & V_{R^*}^{(i)} & P_R^{*(i)} \end{pmatrix},$$
$$U^{(o)} = \begin{pmatrix} H^{(o)} & V^{(o)} & P^{(o)} & P^{*(o)} & R^{(o)} & R^{*(o)} & H_P^{(o)} & V_{R^*}^{(o)} & P_R^{*(o)} \end{pmatrix}. \tag{6}$$

By measuring $U^{(o)}$ experimentally, we have access to the degree of polarization per polarization basis of the output SHG Stokes vector (p_m) and the two-photon Mueller matrix $(M^{(2)})$. The former refers to the elements of a 1×9 degree of polarization row vector (p) obtained by invoking

$$p_m = \frac{\sqrt{U_{m1}^{(o)2} + U_{m2}^{(o)2} + U_{m3}^{(o)2}}}{U_{m0}}, \tag{7}$$

on each column m representing an input polarization state running from 1 to 9. p_m can be thought of as the degree of polarization of the second-harmonic light generated by input polarization state m, after passing through the sample. Also, $U_{m0}^{(o)}$ represents element $m0$ in matrix $U^{(o)}$ (and so on for $m1$, $m2$, and $m3$). Since we have predetermined the input basis, the two-photon Mueller matrix can be determined by solving
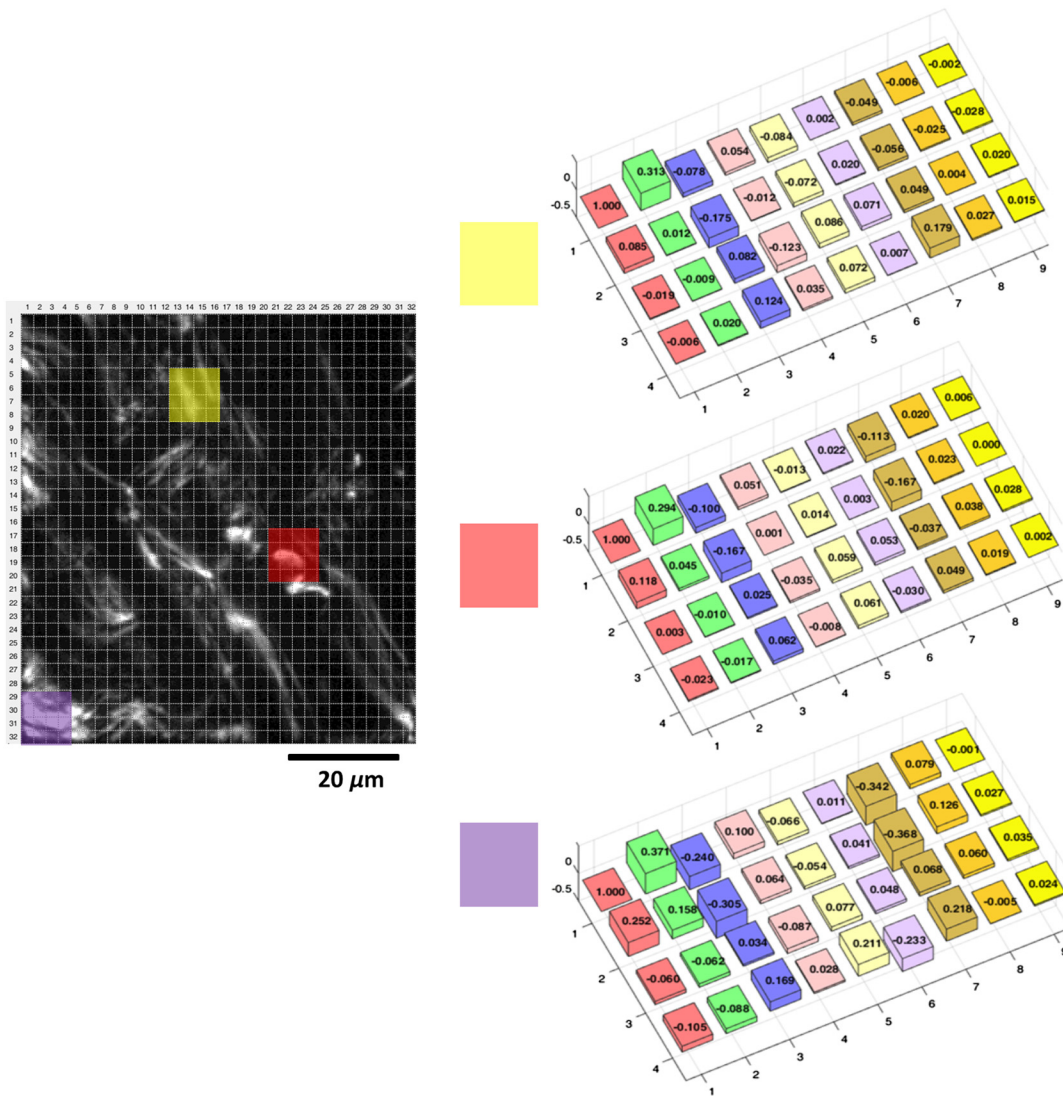
Fig. 3 Sample SHG image of porcine skin showing the division into 32×32 subimage cells using grids. The average $M^{(2)}$ values are shown for select regions in the image, which are highlighted by the colored boxes. The bars for $M^{(2)}(1:1)$ in the bar plots are truncated for visualization convenience.

$$M^{(2)} = U^{(o)} \cdot [U^{(i)}]^{-1}. \tag{8}$$

This approach of obtaining these two metrics can prove useful in understanding how the polarization information may change between different spatial regions within an image.

3 Experimental Setup

Figure 2 shows the experimental setup used. SHG imaging is performed in the forward direction in order to eliminate the use of dichroics which have inferior polarization preserving properties when compared with metal mirrors. A Ti:Sapphire laser (Spectra-Physics Mai-Tai HP DeepSee) produces 100-fs pulses at an excitation wavelength centered spectrally at 780 nm and a repetition rate of 80 MHz. Galvanometer-based scanning mirrors (Thorlabs GVS012) are used to sweep the beam over a rectangular field of view at the sample plane. Polarization states are generated using a polarization state generator (PSG) system comprising a linear polarizer and wave plate combination (half-wave plate for linearly polarized input, quarter-wave plate for circularly polarized input, and both for elliptically polarized input). The beam is then reflected off a metal mirror toward the condenser (0.65NA Olympus 40× PLAN N) which focuses onto the sample. The forward-emitted signal is collected by an infinity-corrected objective (0.8 NA Olympus 50× MPlan FL N) and relayed towards a tube lens for focusing. It should be noted that the condenser lens numerical aperture (NA) was chosen to be low enough (<0.7 NA[18]) to still ignore transverse polarization changes at focus while maintaining an acceptable resolution (which increases with higher NA). Polarization analysis is performed using a polarization state analyzer (PSA) system having a quarter-wave plate and linear polarizer combination. A laser blocking short-pass filter (Semrock FF01-680/SP-25) is used for illumination rejection, while an SHG band-pass filter (Semrock FF01-390/BP-18-25) is used for narrow band filtering. The detector is an electron multiplying charge-coupled device (Hamamatsu EMCCD C9100-13) camera having a gain of 200× and an exposure time of 1 s.

4 Results

Porcine tissue samples were obtained from a local market and embedded in optimal cutting temperature (OCT) compound at −80°C. Next, the samples were brought to −20°C, and cut into
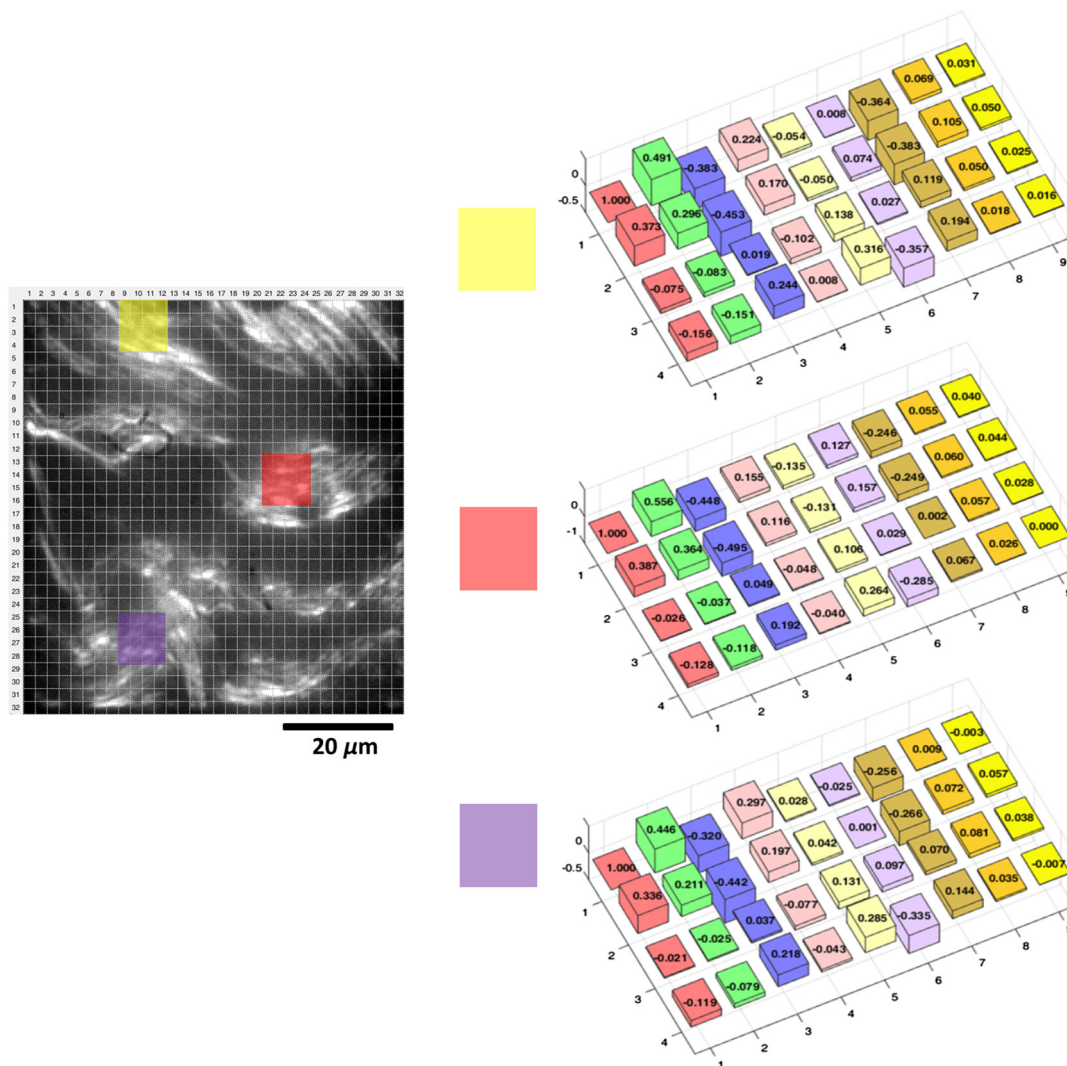
Fig. 4 Sample SHG image of porcine tendon showing the division into 32 × 32 subimage cells using grids. The average $M^{(2)}$ values are shown for select regions in the image, which are highlighted by the colored boxes. The bars for $M^{(2)}(1:1)$ in the bar plots are truncated for visualization convenience.

thin sections using a cryostat (Leica CM3050S). The tissue slices were then soaked in 1× PBS to remove excess OCT, and mounted onto microscope coverslips using aqueous mounting media. Tendon samples at 5, 25, and 75 μm, and skin sample at 5 μm were obtained this way and used in the study.

A set of 54 images, each corresponding to a combination of six PSA states for each nine PSG state, is obtained. We divide an image into smaller "subimage" cell regions, so that if, e.g., a 320×320 pixel image is divided into 32×32 subimage cells using a grid, each subimage cell is a 10×10 pixel image. This is done so that the analysis can be localized and more spatially sensitive. The choice of subimage cell dimension is made based on sensitivity requirements and computational cost. We subsequently determine the local output Stokes vector, degree of polarization per basis and two-photon Mueller matrix within each of these smaller cells using Eqs. (6) and (8).

The analysis is applied to 32×32 subimage cells of two porcine sample types (skin and tendon) at 5-μm thickness. Figures 3 and 4 show SHG images of porcine skin and tendon samples, respectively, with representative average $M^{(2)}$ values over selected localized regions highlighted. We observe that for both samples, there is little sensitivity to mode S_8 [represented in terms of a single Stokes vector by $s_3(s_1 + s_0)$] since the $M^{(2)}(r:9)$ terms (where r stands for the index and runs through all the rows) are negligible compared with the other elements of the matrix. It is noted that this also holds true to a lesser extent for the $M^{(2)}(r:8)$ terms.

In order to investigate the effect of thickness, another study was conducted for porcine tendon samples at 5, 25, and 75 μm.

The values of p_m across the various subimages are obtained, and the results represented as a histogram distribution plot. For a quantitative description, we choose to fit our data to a bimodal model f with normal distribution curves as given by

$$f = q \frac{1}{\sigma_1 \sqrt{2\pi}} e^{-\frac{(p-\mu_1)^2}{2\sigma_1^2}} + (1-q) \frac{1}{\sigma_2 \sqrt{2\pi}} e^{-\frac{(p-\mu_2)^2}{2\sigma_2^2}}, \quad (9)$$

where (μ_1, μ_2) represent the bimodal mean values, (σ_1, σ_2) stand for the bimodal standard deviation values, and $(q, 1-q)$ are mixture probability weights attached to the modes of the distribution. A new metric, the bimodal mean difference μ_d (defined by $|\mu_1 - \mu_2|$), which can be considered a measure of shape distribution, is then retrieved.

For the set of experiments involving the nine input states, input polarization state R (or R-input) shows the greatest variation in μ_d. The R-input results for 32×32 subimage cells across three different spatial regions each for 75-, 25-, and 5-μm thick porcine tendon samples are shown in Fig. 5. Using the bimodal distribution equation, a best fit curve for the histogram is obtained and μ_d extracted. We find here a variation in μ_d (average of 0.068 for 5 μm, 0.150 for 25 μm, and 0.238 for 75 μm), which depends on the thickness. This can be thought of as implying that the thicker the sample, the greater the range of p values and the larger the μ_d values that are obtained from the generated SHG. Qualitatively, this suggests that thicker samples mean more scattering events, and hence greater variation in derived parameters. However, it is important not to draw too
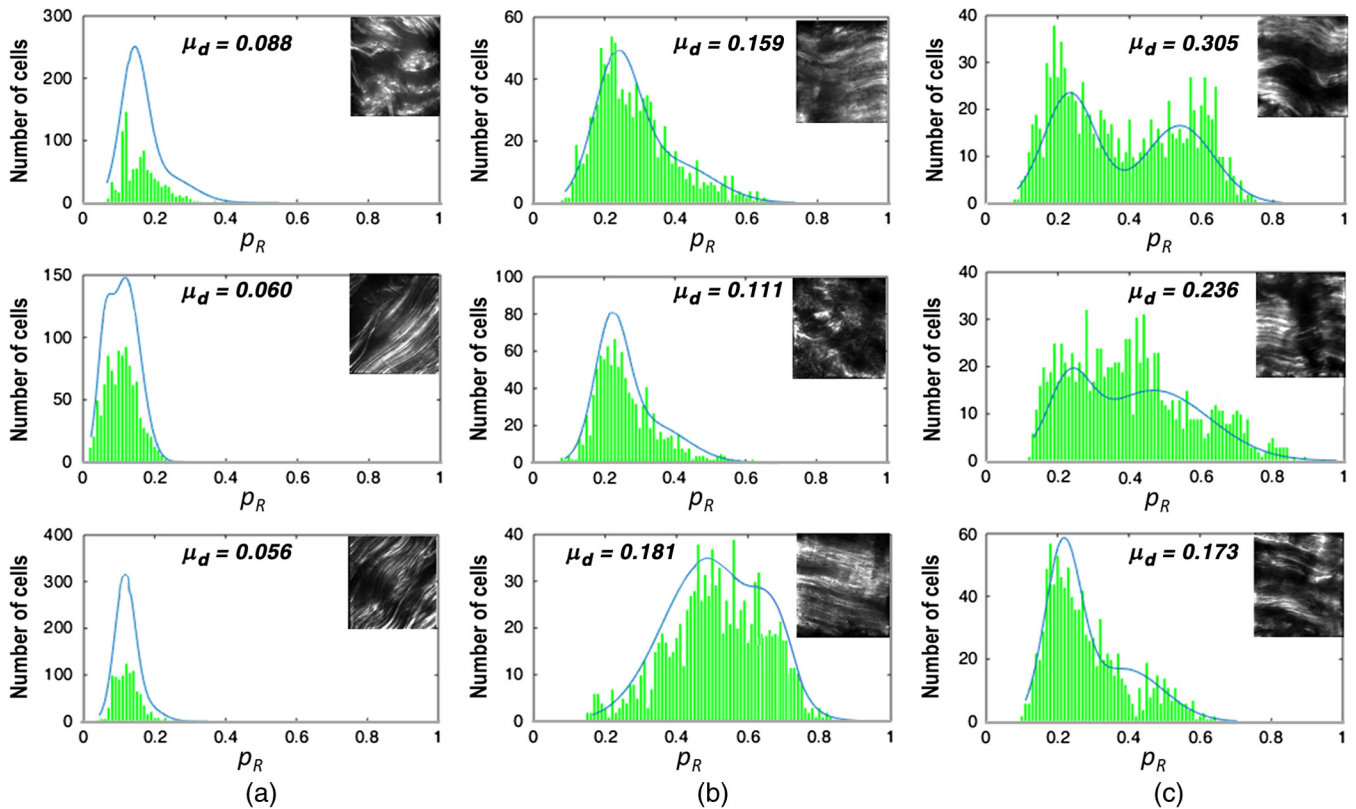
Fig. 5 Histogram plots of p with R-input for porcine tendon at (a) 5 μm, (b) 25 μm, and (c) 75 μm, each taken at three different spatial regions. The solid lines are best fits using the bimodal distribution equation. The associated bimodal mean difference (μ_d) is also provided. Inset for each plot shows SHG images of the different spatial regions. The scale bar above the top left image is 40 μm.

much meaning from these results due to the limited sample size. Rather, the significance of the measurements is that they are robust and permit the inclusion of polarimetry with SHG imaging.

In conclusion, we have carried out what is, to our knowledge, the first experimental demonstration of $MM^{(2)}$-SHG microscopy in extracting the nonlinear Mueller matrices for quantitative assessment of SHG images. Specifically, we experimentally measure the output Stokes vector and use this to determine the two-photon Mueller matrix and degree of polarization. Moreover, we derived another metric, the bimodal mean difference (μ_d), from the degree of polarization distribution model and observed that this metric showed increasing variation with thickness of porcine tendon samples. The increased variation is consistent with the intuition of increased scattering for thicker samples. This can possibly be used in investigating localized growth and/or changes in organizational structure as an indication of abnormality in tissues. However, we note that care should be taken in extracting meaning from p_m because the nonlinearity of SHG complicates relating it to the depolarization of the input Stokes vector. Moving forward, we are currently exploring the computational mining of information-rich two-photon Mueller matrix to obtain additional metrics that would be consistent with a second-order nonlinear scattering process. Furthermore, a multimodal approach can be developed by taking the fiber orientation into consideration, using for example FT-SHG.[8] We believe that our approach can be adapted to other multiphoton coherent imaging techniques.

References

1. T. Y. Lau et al., "Application of Fourier transform-second-harmonic generation imaging to the rat cervix," *J. Microsc.* **251**, 77–83 (2013).
2. R. Ambekar et al., "Quantifying collagen structure in breast biopsies using second-harmonic generation imaging," *Biomed. Opt. Express* **3**, 2021–2035 (2012).
3. B. R. Masters et al., *Handbook of Biomedical Nonlinear Optical Microscopy*, Oxford University Press, New York (2008).
4. M. Winkler et al., "High resolution three-dimensional reconstruction of the collagenous matrix of the human optic nerve head," *Brain Res. Bull.* **81**(23), 339–348 (2010).
5. R. LaComb et al., "Phase matching considerations in second harmonic generation from tissues: effects on emission directionality, conversion efficiency and observed morphology," *Opt. Commun.* **281**, 1823–1832 (2008).
6. R. A. R. Rao et al., "Quantitative analysis of forward and backward second-harmonic images of collagen fibers using Fourier transform second-harmonic-generation microscopy," *Opt. Lett.* **34**, 3779–3781 (2009).
7. R. A. Rao, M. R. Mehta, and K. C. Toussaint, "Fourier transform-second-harmonic generation imaging of biological tissues," *Opt. Express* **17**, 14534–14542 (2009).
8. T. Y. Lau, R. Ambekar, and K. C. Toussaint, "Quantification of collagen fiber organization using three-dimensional Fourier transform-second-harmonic generation imaging," *Opt. Express* **20**, 21821–21832 (2012).
9. X. Han et al., "Second harmonic properties of tumor collagen: determining the structural relationship between reactive stroma and healthy stroma," *Opt. Express* **16**, 1846–1859 (2008).
10. Y. Han et al., "Polarization-sensitive sum-frequency generation microscopy of collagen fibers," *J. Phys. Chem. B* **119**(8), 3356–3365 (2015).
11. T. Hompland et al., "Second-harmonic generation in collagen as a potential cancer diagnostic parameter," *J. Biomed. Opt.* **13**(5), 054050 (2008).
12. C. Brosseau, *Fundamentals of Polarized Light*, John Wiley and Sons, Inc., New York (1998).
13. N. Mazumder et al., "Polarization-resolved second harmonic generation microscopy with a four-channel Stokes-polarimeter," *Opt. Express* **20**, 14090–14099 (2012).
14. F. J. Ávila, O. del Barco, and J. M. Bueno, "Mueller-matrix second harmonic microscopy of collagen-based tissues," in *Focus on Microscopy*, (2015).
15. Y. Shi, W. M. McClain, and R. A. Harris, "Generalized Stokes-Mueller formalism for two-photon absorption, frequency doubling, and hyper-Raman scattering," *Phys. Rev. A* **49**, 1999–2015 (1994).
16. W. H. McMaster, "Polarization and the Stokes parameters," *Am. J. Phys* **22**(6), 351 (1954).
17. M. Samim, S. Krouglov, and V. Barzda, "Double Stokes Mueller polarimetry of second-harmonic generation in ordered molecular structures," *J. Opt. Soc. Am. B* **32**, 451–461 (2015).
18. H. Kang, B. Jia, and M. Gu, "Polarization characterization in the focal volume of high numerical aperture objectives," *Opt. Express* **18**, 10813–10821 (2010).

Chukwuemeka Okoro is a doctoral candidate in the Department of Electrical and Computer Engineering at University of Illinois at Urbana Champaign (UIUC). He has a masters degree in electrical engineering from UIUC and a bachelors degree in electrical engineering from University of Lagos, Nigeria. His current work involves developing quantitative second harmonic generation imaging technique as a tool for assessing biological tissues.

Kimani C. Toussaint Jr. is an associate professor in the Department of Mechanical Science and Engineering, and an Affiliate in the Departments of Electrical and Computer Engineering, and Bioengineering at the University of Illinois at Urbana-Champaign. He directs an interdisciplinary lab which focuses on developing optical techniques for quantitatively imaging collagen-based tissues, and investigating the properties of plasmonic nanostructures for control of near-field optical forces. He is a senior member in SPIE, OSA, and IEEE.